

www.acsanm.org Article

Scalable and Resilient Etched Metallic Micro- and Nanostructured Surfaces for Enhanced Flow Boiling

Nithin Vinod Upot, Allison Mahvi, Kazi Fazle Rabbi, Jiaqi Li, Anthony M. Jacobi, and Nenad Miljkovic*



Cite This: ACS Appl. Nano Mater. 2021, 4, 6648–6658



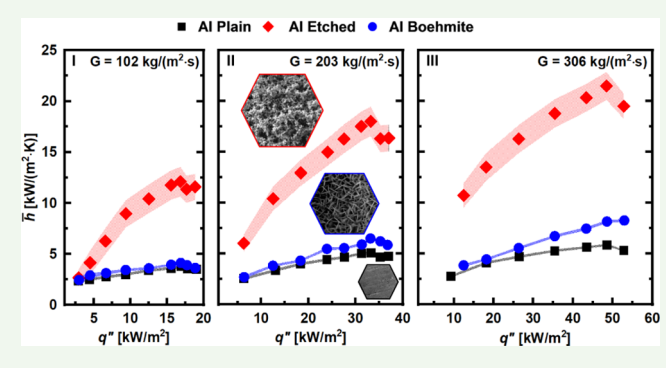
ACCESS

Metrics & More

Article Recommendations

s Supporting Information

ABSTRACT: Flow boiling and evaporation in tubes and channels occur in a wide variety of energy systems, such as refrigeration, air conditioning, power generation, electronics cooling, distillation, and purification. In this work, we demonstrate remarkably increased heat transfer coefficients of 270% during refrigerant flow boiling in scalable microstructured (\sim 40 μ m), industrial-scale (\sim 1 m long) aluminum (Al) tubes, when compared to smooth unstructured Al tubes. To achieve scalable nanomanufacturing, we create highly conformal and durable structured surfaces by relying on hydrochloric acid Al etching. Flow boiling tests were conducted in 6.35 mm diameter Al tubes using R134a refrigerant as the working fluid. To benchmark our approach and to elucidate the



effect of the structure length scale, we also fabricated ultrascalable boehmite (AlO(OH)) nanostructured (~300 nm) Al tubes, showing that etched microscale features are necessary and key to enhancement. Durability tests conducted using a 28 day long continual flow boiling experiment demonstrated negligible degradation of the etched surfaces. The scalable and cost-effective techniques used to create these durable, etched-Al microstructures may significantly reduce manufacturing cost when contrasted with current enhancement approaches such as extrusion, drawing, and welding.

KEYWORDS: microstructure, nanostructure, scalable, flow boiling, enhancement, durable, etching

■ INTRODUCTION

Flow boiling is ubiquitous to a variety of industrial sectors such as thermal management of electronics, purification, distillation,³ chemical synthesis,⁴ desalination,⁵ thermoelectric power generation, ^{6,7} refrigeration, ^{8–10} and cryogenics ¹¹ since it offers the dual advantage of near-isothermal operation and ultraefficient energy transfer. Although the flow boiling heat transfer coefficient, a characteristic measure of the efficiency of heat transfer, is higher when compared to other modes of thermal exchange such as single phase flow, 12 many researchers and engineers have looked for methods to further enhance the heat transfer coefficient via surface macro-, micro-, and nanostructuring or decreased channel diameter (i.e., microchannels).¹³ For example, the transition of wide band gap semiconductor devices made from gallium nitride (GaN) and silicon carbide (SiC) from lab-scale to industrial platforms, 14,15 coupled with thermal limitations placed on silicon (Si) processor densification, 16,17 has recently renewed the push to develop technologies that are able to safely and reliably transfer ever-higher heat transfer rates. 18,19 To achieve enhancement, past work has developed silicon nanowires and silicon micropillars as a platform technology capable of increasing boiling heat transfer in microchannels with water as the working fluid. For example, the inclusion of silicon nanowires

in silicon microchannel heat sinks causes the early onset of nucleate flow boiling, dampens wall temperature oscillations, and increases the heat transfer coefficient for water at moderate mass fluxes. These properties are the result of the large number of nucleation cavities, the superhydrophilic nature of the nanowires, and the ability to maintain a stable liquid film.²⁰ Similar mechanisms of heat transfer enhancement have also been demonstrated with silicon micropillar arrays in microchannels.²¹ In addition to water, nanowire-covered microchannels also exhibit improved performance with alternative low-surface tension working fluids such as dielectrics.^{22,23} Flow boiling enhancements for low-surface tension fluids have also been demonstrated utilizing refrigerants^{24–26} and surfacealtering techniques.^{27,28} Surface modifications with coatings such as pHEMA,^{29,30} porous structures,³¹ nanocomposites,³² and carbon nanotubes 33,34 have all demonstrated enhanced heat transfer coefficients by up to 180% with a pressure drop

Received: February 19, 2021 Accepted: June 8, 2021 Published: June 21, 2021





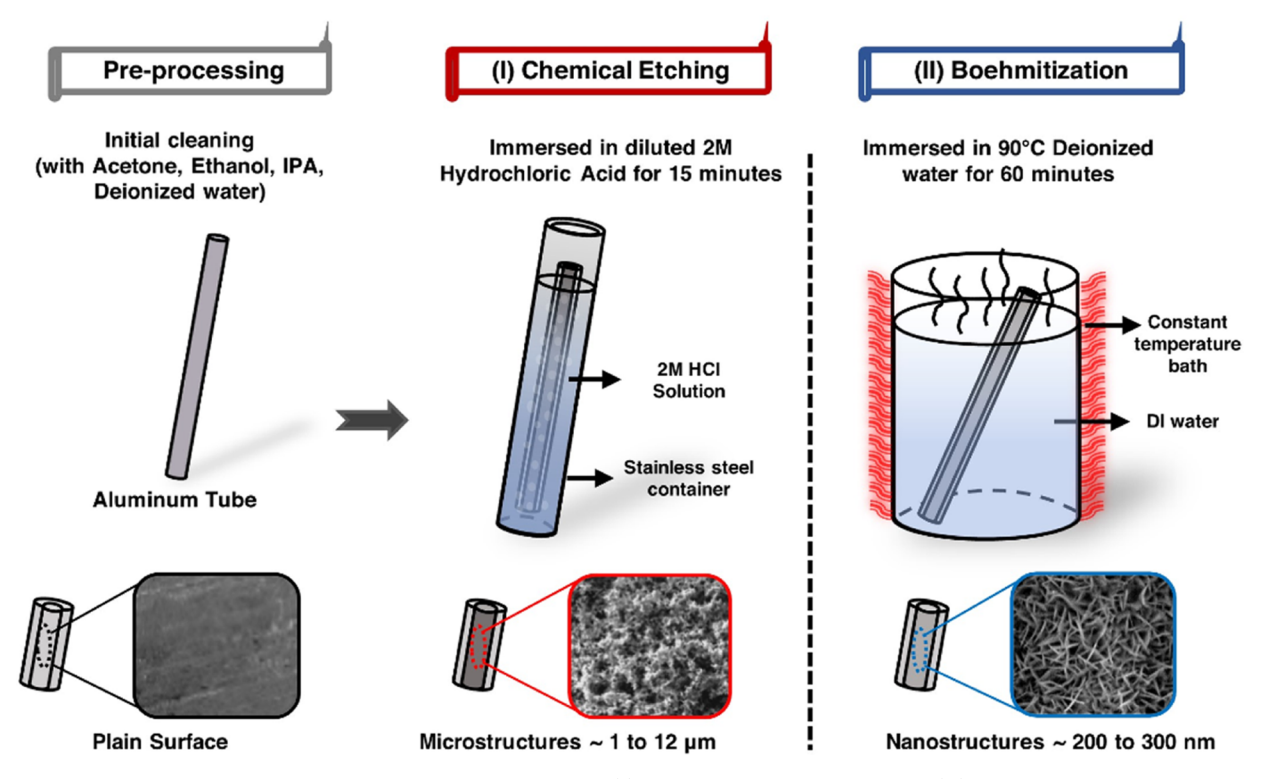


Figure 1. Schematic showing the fabrication procedure developed for (I) microstructured etched Al and (II) nanostructured boehmite. Cleaning procedure adopted for both methods remains the same and is shown in the preprocessing step.

penalty up to 20%. Instead of surface modifications, flow boiling instabilities such as temperature and pressure drop fluctuations can also be addressed with inlet restrictors, wherein the cross-sectional area at the channel inlet is reduced.³⁵ If such surface and geometry modifications are employed while maintaining a low pressure drop, they can lead to highly compact and efficient systems ideal for high-power-density applications.

While structured microchannels can significantly improve heat transfer coefficients, the requirement of flow splitting between multiple small-diameter channels to maintain reasonable pressure drops increases the complexity and introduces the potential for flow maldistribution. Furthermore, the majority of surface structuring techniques developed over the past decade to enhance flow boiling are difficult or impossible to scale, ²¹ not characterized in terms of durability, ³⁶ difficult to manufacture on typical heat exchanger materials, ³³ or have been typically studied with fluids such as water or dielectric fluids at ambient pressure. ³⁷ Limited research exists in developing ultrascalable technologies to augment two-phase flow heat transfer in conventional millimetric-scale channels relevant to the majority of energy systems.

In this study, an ultrascalable, superhydrophilic, cost-effective, simple, and highly durable surface structuring technique for Al substrates using crystallographic hydrochloric acid (HCl) etching is demonstrated. The crystallographic etching technique to develop structures has three main advantages. First, the structure length scale for etched Al is larger than the majority of considered structures in the past, enabling greater structure strength and resilience to external forces such as shear and abrasion when compared to fragile nanostructures. Second, crystallographic etching of Al results in an all-Al structured surface that is intricately connected to the Al substrate with no additional oxide layer or interface. This

results in the elimination of interfacial stresses and failure modes such as delamination, interfacial cracking, and blistering.⁴⁰ Finally, common oxidation methods to enhance heat transfer are sensitive to the chemistry of the working fluid. 41 Slight acidity in the working fluid can result in the reduction of the structures and failure of the enhancement. To examine the role of the structure length scale on the flow boiling performance, we compare our samples to welldeveloped nanoscale hydrophilic structures (boehmite). We quantify the flow boiling performance in a custom-built experimental facility with a hydrofluorocarbon refrigerant 1,1,1,2-tetrafluoroethane (R134a) as the working fluid. The results demonstrate enhanced flow boiling thermal performance in microstructured conventional 1 m long Al tubes. Nanostructures are conclusively shown to have a negligible effect on the flow boiling performance. Experiments carried out over a range of heat flux and mass flux conditions revealed heat transfer coefficient enhancement up to 270% for etched surfaces when compared to plain Al tubes with similar pressure drop characteristics. To demonstrate the scalability of our approach and ability to coat complex internal features with ease, we demonstrate conformal Al etching of commercially available 9.5 mm (3/8") diameter low-fin tubing, indicating potential enhancements approaching more complex and expensive modification techniques such as extrusion, drawing, and welding. Additionally, we performed a continual 28 day flow boiling test to investigate preliminary structure durability, demonstrating negligible change in heat transfer performance over the entire test duration.

RESULTS AND DISCUSSION

Surface Characterization. The baseline tubes in these experiments are commercially available 1/4'' plain Al tubes with outer diameters of $D_{\rm out}$ = 6.35 mm, inner diameters of $D_{\rm in}$

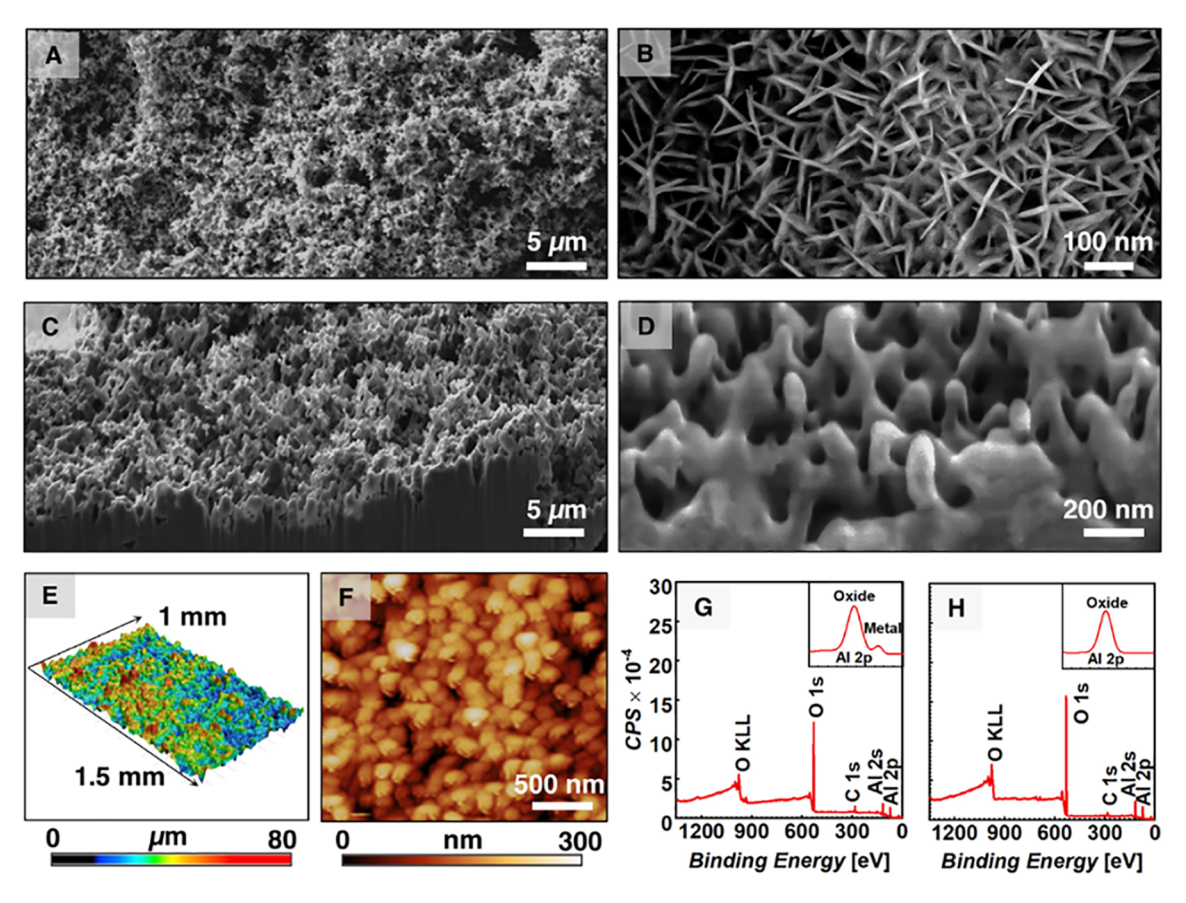


Figure 2. SEM of (A) etched Al and (B) boehmite, along with the corresponding FIB milling images identifying the height of each roughness feature as (C) 5 μ m for etched Al and (D) 100 nm for boehmite. Roughness profiles for (E) etched Al determined using confocal microscopy, and (F) boehmite structures using AFM. XPS spectra confirmed material composition for (G) etched Al and (H) boehmite.

= 3.048 mm, and lengths of $L=90\pm0.1$ cm. The test-section length was chosen for two reasons: (1) to demonstrate the scalability of the technique for micro-/nanostructure fabrication on the internal surfaces of long tubes and (2) to enable the transition from fully single-phase liquid flow to fully single-phase vapor flow inside a single test section. While numerous definitions exist for the classification of channels as micro/mini/conventional, we classify our tubes as conventional, with two distinct structure length scales: microscale Al (~40 μ m) and nanoscale Al (~300 nm).

The cleaning procedure used for fabricating both tube samples was identical. The tube was first dipped in acetone for 5 min to remove organic materials and then was cleaned with ethanol, isopropanol, and deionized (DI) water in succession (see Section S1 for fabrication details). The HCl-etching process on the internal surface of the tube is shown in Figure 1I. A 1 in. diameter stainless-steel (SS) tube was used as a container with one end closed with a rubber stopper. The SS tube was filled with 500 mL of 2 M HCl. The Al tube was wrapped with 1 mm thick Kapton tape to maintain a smooth outer surface and was then placed in the HCl solution and left for 15 min. The inner diameter of the etched tube changes by 0.13 mm, and this tube was finally cleaned with DI water and isopropanol to remove any residue, and the internal surface was dried in air. To create internal boehmite nanostructures (Figure 1II), the SS tube is first filled with DI water. This solution is heated by a rope heater wound around the tube, and the solution temperature was monitored with a T-type thermocouple. Once the temperature reaches 90 °C, the

Kapton-wrapped aluminum tube is immersed in the DI water for about 60 min. The heater is controlled to keep the solution temperature between 90 and 100 $^{\circ}$ C for the duration of the soaking process. The resulting needle-like nanostructured aluminum tube is then removed and dried with a nitrogen stream. ⁴⁵

Figure 2 shows the scanning electron microscopy (SEM), focused ion beam milling (FIB), atomic force microscopy (AFM), and X-ray photoelectron spectroscopy (XPS) analysis of the two fabricated micro/nanostructured surfaces. The etched surface displays two length scales: (1) an \sim 5 μ m structure length observed through FIB and (2) an \sim 40 μ m peak to valley height observed through 3-D optical profilometry. The larger length scale is a result of etching along the aluminum grain boundaries. The etched structures also exhibited the largest cavity sizes (5 μ m), while the boehmite structures have much smaller pores (~45 nm) due to their dense interconnected layout as deduced through SEM images. For the Al samples, Figure 2G,H shows the wideband XPS spectra of Al 2p and O 1s with the expected binding energy revealing the presence of Al and O on the sample surface. The insets of Figure 2G,H illustrate the high-resolution XPS spectra showing the presence of only aluminum oxide on the boehmite surface and both aluminum oxide (native) and Al metal on the etched Al surface. For additional details regarding surface characterization, see Section S3.

Comparative Analysis of Microstructured and Nanostructured Surfaces. The heat transfer performance for the fabricated structures is quantified by measuring the heat

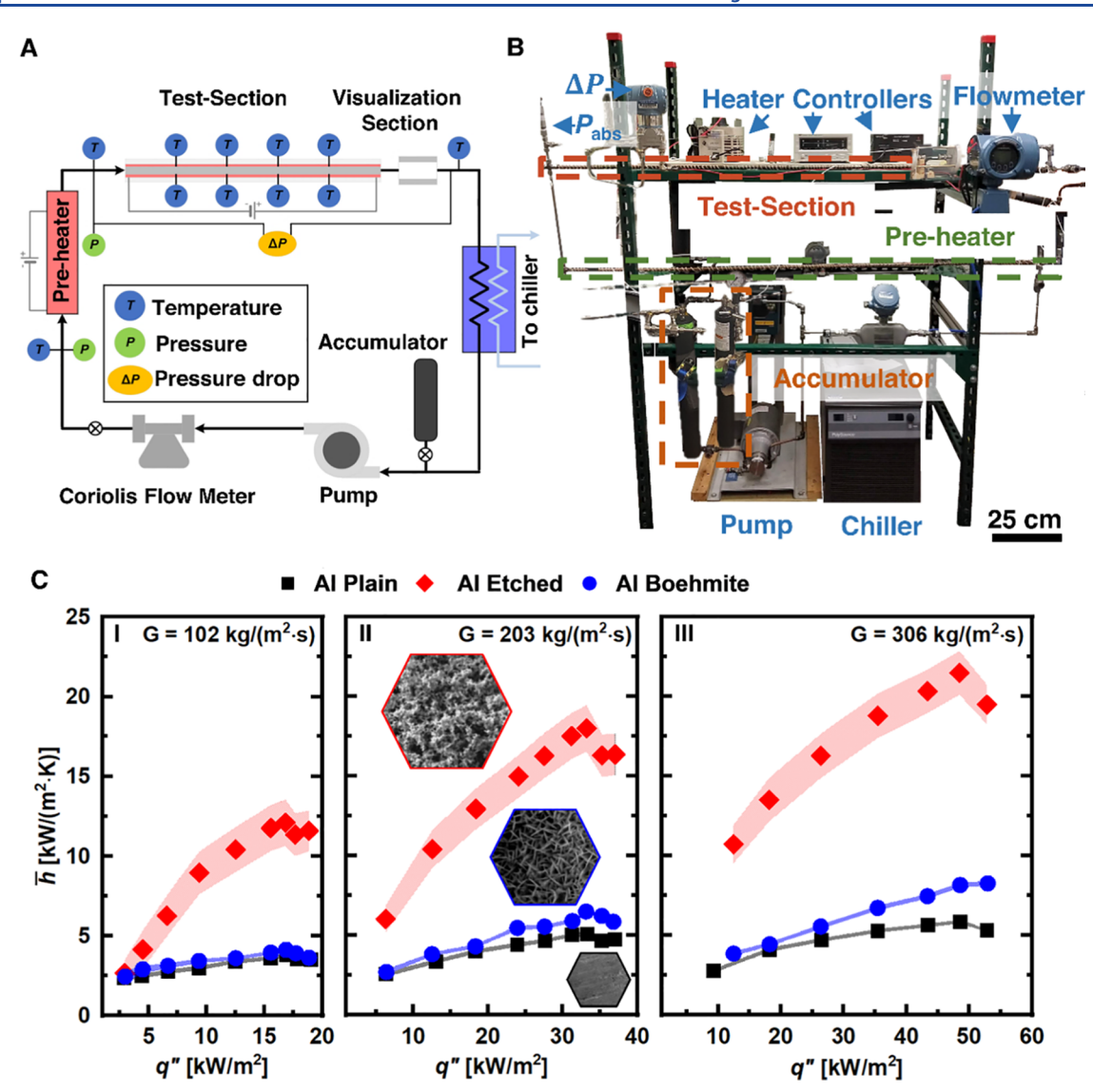


Figure 3. (A) Schematic and (B) photograph of the experimental flow boiling facility showing key instrumentation used to measure temperature (T) and pressure (P). (C) Experimental average heat transfer coefficient (\overline{h}) as a function of heat flux (q'') for R134a flow boiling at mass flux (G) of (I) 102 kg/(m²·s), (II) 203 kg/(m²·s), and (III) 306 kg/(m²·s). The saturation temperatures for (I)–(III) were $T_{\text{sat}} = 30$ °C. Error for \overline{h} has been represented by the shaded region. Error bars for plain and boehmite tubes are smaller than the symbols; however, the shaded region between two data points represents the uncertainty. For further experimental details and uncertainty analysis, see Sections S4 and S5.

transfer coefficient across the test section of interest (fabricated structured tubes and a plain tube as a control), in a custom flow boiling experimental facility (Figure 3A,B). While the majority of past flow boiling work on structured surfaces has focused on water, we characterize refrigerant boiling because of its prevalence in a wide variety of applications where water is inappropriate to use. The refrigerant used for testing was R134a, which is a nontoxic, noncorrosive, and nonflammable alternative to chlorofluorocarbons and hydrochlorofluorocarbons widely used in the automotive, aerospace, pharmaceutical, and manufacturing industry. Prior to flow boiling experiments, the facility was vacuumed to avoid contamination of the working fluid with air. The mass flux was varied between 100 and 300 kg/(m²·s), and the heat flux was adjusted to cover two-phase vapor qualities, the ratio of the mass of vapor to total mass of saturated mixture, from 0 to 1. The mass flux range studied enabled us to traverse multiple flow regimes, which is critical to develop an understanding of the heat transfer performance for both nucleate and convective flow

boiling regimes. The local wall temperature was measured at six locations along the test section by one surface-mounted thermocouple attached to the top and another thermocouple attached at the bottom of the tube at each location. These measurements were used to determine the local heat transfer coefficients, and the mean of these values was reported as the average heat transfer coefficient across the test section. A needle valve was used to mitigate flow boiling instabilities across the test section, while the pressure drop across the test section was recorded using a differential pressure transducer to quantify changes in the required pumping power. Finally, the refrigerant was routed through a glass tube placed 3.8 cm beyond the exit of the test section, and the flow regimes were recorded with a Phantom High-Speed Camera at 5000 frames per second. For further details on the experimental test section, procedure, data reduction, and uncertainty analysis, please refer to Sections S4 and S5.

Nucleate boiling and convective boiling are the two major mechanisms that exist during flow boiling. ⁴⁶ In the nucleate

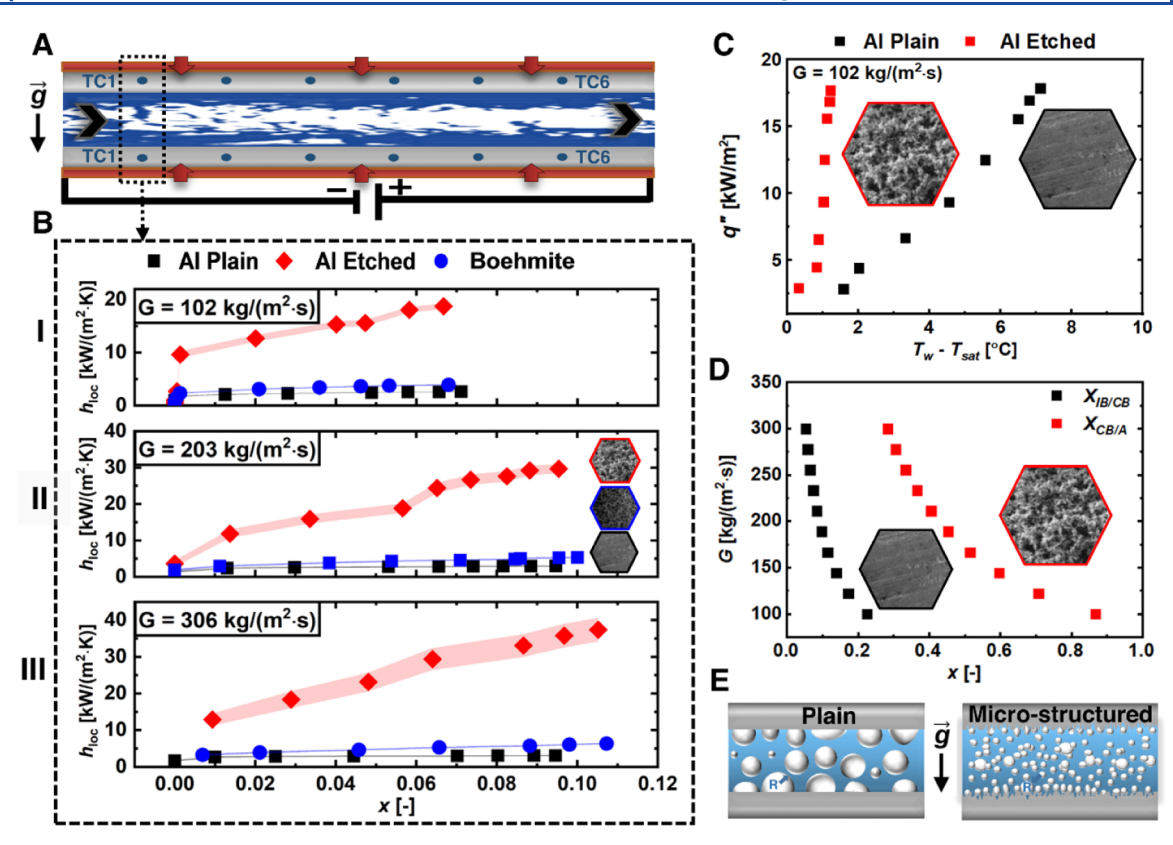


Figure 4. (A) Schematic of test-section showing the location of first thermocouple. (B) Experimentally measured local heat transfer coefficients (h_{loc}) as a function of vapor quality (x) at mass flux (I) $G = 102 \text{ kg/(m}^2 \cdot \text{s})$, (II) $G = 203 \text{ kg/(m}^2 \cdot \text{s})$, and (III) $G = 306 \text{ kg/(m}^2 \cdot \text{s})$. Measurement uncertainty is represented by the shaded region. Error bars for plain and boehmite tubes are smaller than the symbols; however, the shaded region between two data points represents the uncertainty. (C) Heat flux (q'') of the microstructured etched Al tube and plain Al tube as a function of wall superheat $(T_w - T_{\text{sat}})$ at mass flux $G = 102 \text{ kg/(m}^2 \cdot \text{s})$. Error for heat flux (q'') is smaller than the symbol and has not been shown for clarity. (D) Flow regime map identifying transition vapor qualities for isolated bubble (X_{IB}) , coalescing bubble (X_{CB}) , and annular flow (X_A) , at heat flux $q'' = 5 \text{ kW/m}^2$. (E) Schematic of the enhanced nucleation phenomena attributed to increased nucleation site density. Schematics are not to scale.

boiling regime, the heat transfer coefficient is the primary function of the heat flux, with an increasing number of nucleation sites being activated on an increase in supplied heat. However, the heat transfer coefficient is nearly independent of the heat flux in the convective boiling regime. Figure 3C shows the measured average heat transfer coefficients across the length of the test section (\overline{h}) as a function of wall heat flux (q''). For all tested mass fluxes, flow boiling heat transfer enhancement was observed for the porous etched Al tube, with a significant increase in h as a function of q'' pointing toward nucleate boiling dominance across the test section. A maximum increase of 270% for heat transfer coefficient was attained at the highest mass flux case of $G = 300 \text{ kg/(m}^2 \cdot \text{s})$ (Figure 3CIII). A strong correlation between heat flux and heat transfer coefficients at a specified mass flux along with a negligible effect of mass flux on heat transfer coefficients at a specified heat flux (Figure 3CI-III) implies nucleate boiling dominance for the microstructured etched Al surface. A similar negligible mass flux effect is observed for the plain Al and boehmite tubes; however, the effect of heat flux is at a significantly lower scale when compared to the etched tube. Thus, while nucleate boiling dominance is exhibited through flow boiling tests with the three surfaces, the microstructured etched surface demonstrates the greatest nucleate boiling

To gain an understanding of the enhancement mechanisms, local properties were analyzed near the entrance (Figure 4A)

and exit of the test section. Figure 4B shows the local heat transfer coefficients ($h_{\rm loc}$) at the location closest to the tube inlet as a function of the local vapor quality (x), which was varied by increasing the applied heat flux at a constant mass flux G. Significantly higher heat transfer coefficients are demonstrated for the microstructured Al etched tubes at all tested mass flux values. This is attributed to a dominance of nucleate boiling, an increase in the number of active nucleation sites, and an increase in the bubble departure frequency.

To model the nucleation site density, we used a formulation based on parameters such as degree of subcooling, wall superheat, and apparent contact angle.⁴⁷ Our analysis found the length scale of active nucleation sites to range between 0.08 and 12 μ m (see Section S8). The increase in local heat transfer coefficients by 10 times for the etched Al tube at the highest mass flux (Figure 4BIII) is attributed to the higher density of microcavities in the desired range (\sim 5 μ m diameter), with boiling being sustained at lower wall superheats. The same mechanism of enhancement applies to the lower mass fluxes as well. An increase in heat flux leads to the activation of more nucleation sites, resulting in the higher heat transfer coefficients as observed in Figure 4BI-III for all examined surfaces and for all mass flux values. When compared to the plain Al tube, nanostructured boehmite surfaces also showed an improvement due to the increase in nucleation sites, but the enhancement was well below the enhancement obtained with the microstructured etched Al surface. The lack of substantial

ACS Applied Nano Materials

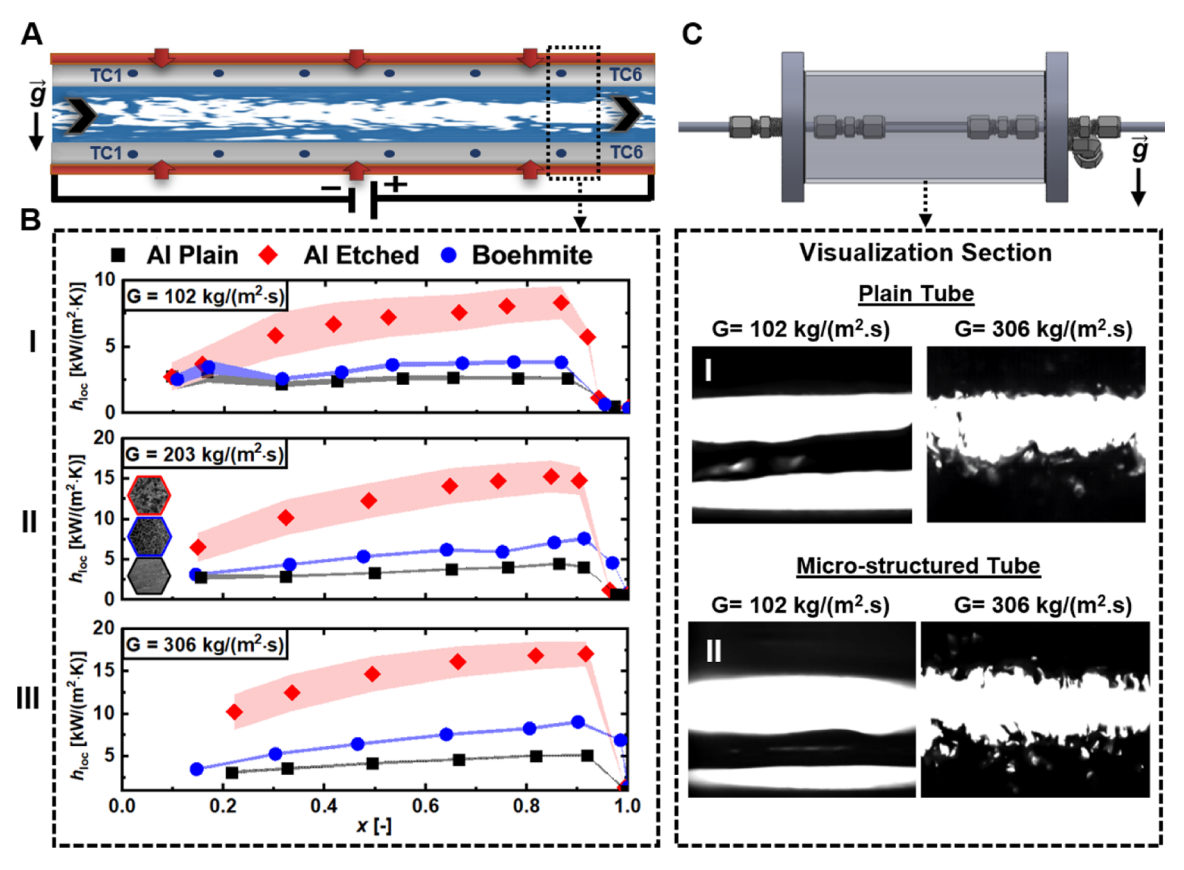


Figure 5. (A) Schematic of the test section showing the location of the last thermocouple. (B) Experimentally measured local heat transfer coefficient (h_{loc}) as a function of vapor quality (x) at a mass flux of (I) $G = 102 \text{ kg/(m}^2 \cdot \text{s})$, (II) $G = 203 \text{ kg/(m}^2 \cdot \text{s})$, and (III) $G = 306 \text{ kg/(m}^2 \cdot \text{s})$. Error for h_{loc} has been represented by the shaded regions. Error bars for plain and boehmite tubes are smaller than the symbols; however, the shaded region between two data points represents the uncertainty. (C) Flow regime visualization recorded at test-section exit displaying a lower liquid film thickness for the microstructured etched Al tube in the stratified wavy regime (CI) at $q'' = 9 \text{ kW/m}^2$ and an annular flow regime at $q'' = 43 \text{ kW/m}^2$ (CII).

enhancement is attributed to the smaller cavity size of the boehmite surface (~45 nm) in comparison to the etched Al surface (Figure 2). Care must be taken to optimize the cavity size for the working fluid of interest as there exists a maximum cavity diameter for heterogeneous nucleation, beyond which nucleation is suppressed. The nucleation suppression occurs due to subcooled liquid flooding on surfaces with cavities that are too large, which leads to the suppression of vapor entrapment in the pores. The effect of flooding is even more detrimental for low surface tension fluids such as R134a, the working fluid under consideration here, due to the smaller volume of gas entrapment when compared with high surface tension fluids such as water. 48 The cavity depth also plays an important role in nucleation. The deeper cavities on the etched Al surface in comparison to the boehmite surface (40 μ m vs 300 nm) enables greater vapor entrapment in the pores, further enhancing heat transfer. Therefore, the combined effects of increased cavity diameter and depth of the microstructured Al etched surface lead to significantly enhanced flow boiling near the test-section inlet.

The dominance of nucleate boiling near the entrance of the etched tubes can be seen via analysis of the boiling curve in Figure 4C. Beginning at \sim 0 °C, the wall superheat varies linearly with heat flux for the plain tube, implying convective boiling dominance due to the independence of heat transfer coefficient on heat flux. However, a nonlinear trend is observed for the microstructured etched surface, implying a transition

from the convective to the nucleate boiling regime.⁴⁹ Similar nonlinear trends for the microstructured Al surface hold for high mass fluxes.

Flow patterns have previously been shown to affect heat transfer coefficient values, and numerous flow regime maps exist to identify local regimes and threshold criteria for transition between flow regimes. 50,51 As shown in Figure 4D, an appropriate flow regime map (see Section S9) was chosen to identify the regime near the entrance of the test section. 52,53 Nucleation and the resulting bubbles formed drive the thermal performance in this region of high heat transfer enhancement at low vapor qualities (x < 0.1). Concentrating on the bubble characteristics (Figure 4E), an increase in the rate at which bubbles depart from the surface, known as the bubble departure frequency (f),54 contributes to an increase in heat transfer during nucleate boiling. The duration of bubble growth is dependent on the time required for the bubble to reach departure diameter size, and therefore, the departure frequency is inversely proportional to bubble departure diameter (D_d) . The departure diameter is in turn related to the wettability of the surface and the magnitude of drag force assisting bubble departure during flow. The bubble departure diameter D_d of the high roughness Al etched surface decreases with contact angle ($\theta \sim 0^{\circ}$) (see Section S10) since $D_{\rm d} \sim \theta [\sigma/g(\rho_{\rm l}-\rho_{\rm v})]^{1/2}$, where θ is the apparent receding contact angle as measured between the liquid-vapor interface and solid–liquid interface, σ is the working fluid liquid–vapor

surface tension, g is the gravitational constant, and ρ_1 and ρ_v are the working fluid liquid and vapor densities, respectively. S5,56 In addition, the drag and inertia forces during flow balance the capillary force (F_c) , which is the force keeping the bubble attached to the wall. The capillary force ($F_c = \pi D_d \sin \theta$) reduces with increased wetting associated with etched surfaces and therefore enables bubbles to depart the surface at smaller diameters and results in higher heat transfer coefficients. With regard to the average heat transfer coefficient, plain and boehmite surfaces showed similar behavior with the exception of the highest mass flux case ($G = 300 \text{ kg/(m}^2 \cdot \text{s})$), where the boehmite tube exhibited a slightly better performance, showing a 17% increase in \overline{h} (Figure 3CIII).

While the greater performance enhancement toward the beginning of the test section is attributed to enhanced nucleation characteristics, a large portion of the test section is in the coalescing bubble/annular flow regime. Because of the suppression of nucleate boiling at higher vapor qualities, the degree of heat transfer enhancement toward the end of the test section (Figure 5A) for the microstructured etched Al surface is of a significantly lower magnitude when compared to that observed toward the beginning of the test section. As an example, the local heat transfer coefficient is 3 times higher than that for the plain surface at the highest mass flux case (Figure 5BIII). To better understand the mechanism of heat transfer in this regime, the heat transfer and flow regime characteristics (Figure 5B,C, respectively) were examined near the test-section exit. At low mass flux $(G = 100 \text{ kg/(m}^2 \cdot \text{s}))$ where phase velocities are low, stratified flow was observed at the exit of the test section where both liquid and vapor are separated into two distinct regions with the liquid occupying the bottom of the tube due to gravity (Figure 5CI). At higher mass flux ($G > 200 \text{ kg/(m}^2 \cdot \text{s})$), an increase in the vapor flow rate results in annular flow where liquid wets the tube around the periphery of the tube wall with a central vapor core (Figure 5CII).

A high-speed video comparison of annular flow regimes for plain and microstructured surfaces indicates an increase in the turbulence for the etched surface, attributed to an increase in cavity distribution (see Section S11 and Video S1). Enhanced turbulence results in improved vapor removal from the heated surface as well as increased mixing of cold liquid from the bulk toward the heated surface, 57 both of which contribute to improved heat transfer. In addition, the flow regime characteristics also depend on the nondimensional capillary number, which represents the ratio of the viscous force to the surface tension force. The plain tube has an approximately 6% higher capillary number when compared to the structured tubes; hence, the plain tube should have a thicker film. This was confirmed for the stratified flow regimes using the recorded visualization images. Thinner films lead to a lower conduction resistance across the liquid, resulting in higher heat transfer coefficients for the etched tube toward the end of the test section. Thus, while the heat transfer enhancement is lower near the end of the test section, the etched tube still shows benefit due to the significant increase in turbulence in annular flow and marginal reduction in liquid film thickness in stratified

Because of the sudden increase in the wall temperature associated at high vapor qualities, dry-out is another important parameter that needs to be considered. Partial dry-out is defined as the region in which intermittent wetting and

rewetting of fluid in the periphery of the tube wall occurs and is found to occur at a vapor quality of approximately 0.9. This value increases with increasing mass flux for both structured and unstructured tubes due to an increase in the amount of heat that needs to be supplied to reach the specified vapor quality. While prior studies have reported enhancements in dry-out completion with water as the working fluid, ⁵⁸ no significant improvement in partial dry-out was observed in this study, primarily due to the low liquid—vapor surface tension working fluid being considered ($\sigma = 8 \text{ mN/m}$ for R134a when compared to $\sigma = 72 \text{ mN/m}$ for water at room temperature).

While many prior studies focused on flow boiling enhancement have not reported pressure drop, 20,37 it is important to consider since it gives a measure of the pumping cost and changes in the saturation temperature associated with the observed enhancements. Figure 6A shows the comparison of pressure drop across the test section for the micro-/ nanostructured tubes with the unstructured plain Al tube. The pressure drops across all the tubes increased with heat flux because of the higher vapor qualities present. As expected, the two-phase pressure drop for the microstructured Al tube is close to 10% higher due to the largest features and highest roughness among the tested surfaces. To quantify the advantageous nature of the fabricated etched Al surface, an enhancement factor, which incorporates the average heat transfer enhancement and total pressure drop, is used and defined as $\phi_{\rm e.f.} = (\overline{h}_{\rm structured}/\overline{h}_{\rm plain})/(\Delta P_{\rm structured}/\Delta P_{\rm plain})^{.59}$ The enhancement factor is always greater than 2 and peaks at $\phi_{\text{e.f.}}$ = 3.15 (Figure 6B), indicating that the detrimental impact of a pressure drop increase is offset by a higher increase in heat transfer coefficients.

Enhanced Durability and Microstructuring of Enhanced Surfaces. Prolonged sustainability of previously designed micro-/nanostructures for flow boiling enhancement remains a concern.⁶⁰ To demonstrate the applicability of the internal microstructured etched Al surface for commercial flow boiling applications, we examined a preliminary durability study of the surface by conducting daily 8 h long two-phase heat transfer experiments for a total of 28 days. The microstructures formed on the surface of aluminum are through crystallographic chemical etching of the base metal. Because of the absence of a significant oxide layer, shear stress is minimized at the metal-oxide interface when subjected to flow. This in turn results in highly stable structures, as confirmed through steady experimental heat transfer coefficient results over time (Figure 6C). The proven structural integrity of the microstructured etched surface points to their possible use for longer time periods typically encountered in industrial applications. In contrast, the presence of an oxide layer in the fabricated boehmite structures can make these surfaces prone to wear during flow and thermal cycling, primarily due to the thermal expansion coefficient mismatch between the oxide layer and base metal. Thus, in addition to advantages highlighted earlier with regards to thermal performance, chemically etched microstructures can also lead to favorable mechanical properties during two-phase flow. It must also be noted that since there is no specialized equipment requirement for the structure fabrication methods described in this study, the preparation cost is mainly related to the chemical reagent cost. The estimated lab-scale manufacturing cost for etched Al tube reduces to as low as \$7/m², which is lower than the majority of alternate structure fabrication methods described in the literature such as sintering, nanowire growth, and **ACS Applied Nano Materials**

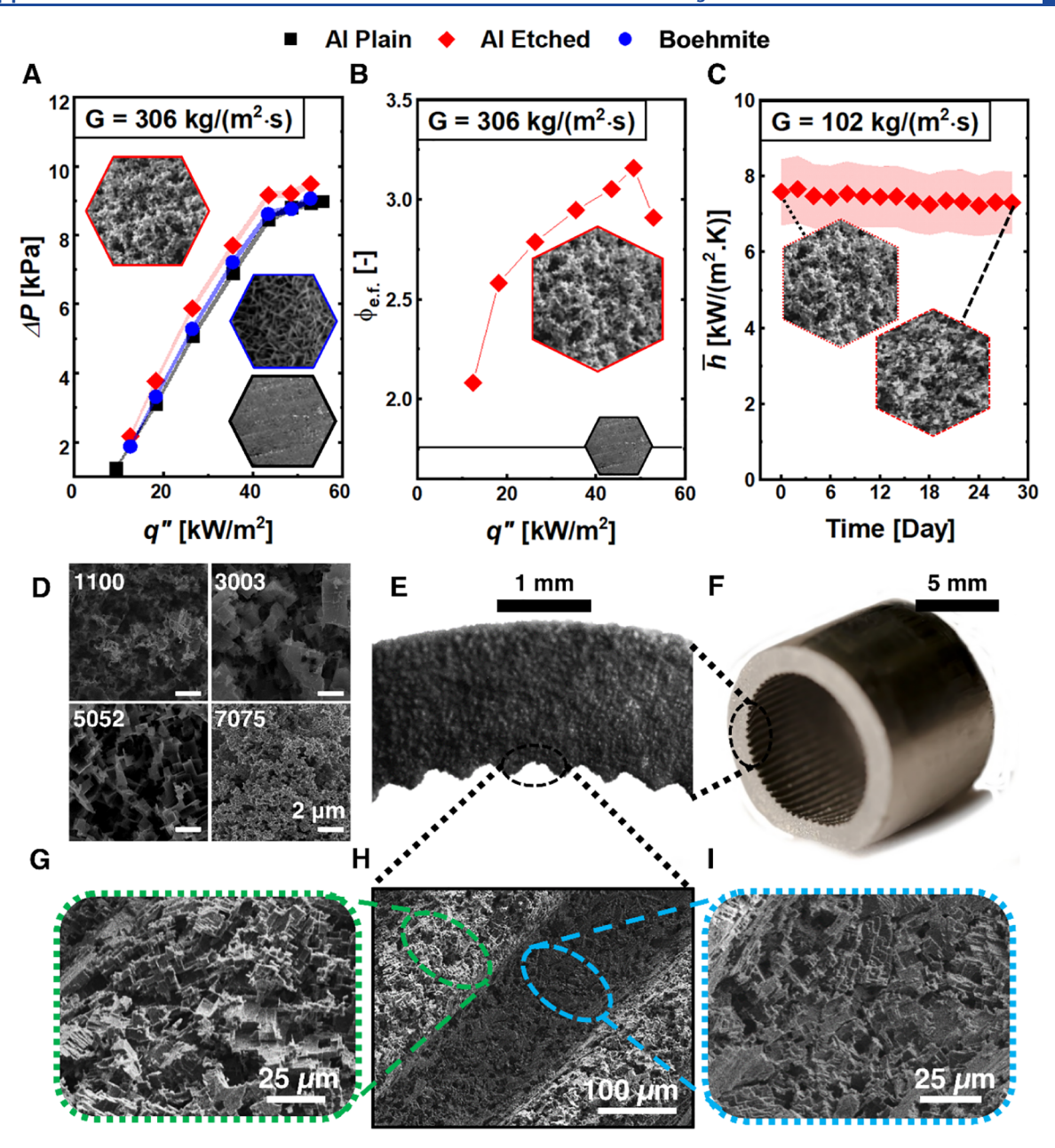


Figure 6. (A) Pressure drop comparison between a microstructured etched Al tube, nanostructured boehmite tube, and a plain tube at a mass flux $G=306~{\rm kg/(m^2 \cdot s)}$. (B) Enhancement factor $(\phi_{\rm e.f.}=(\overline{h}_{\rm structured}/\overline{h}_{\rm plain})/(\Delta P_{\rm structured}/\Delta P_{\rm plain}))$ for etched Al tube. (C) Measured heat transfer coefficient (\overline{h}) as a function of time over a period of 28 days, showing negligible change and indicating structure durability. Insets showing similar SEM images before and after flow boiling tests confirm structure durability. (D) SEM images showing microstructure formation on various industrial Al grades. (E) Zoomed-in view of a sectioned 9.5 mm diameter etched extruded Al grooved tube. (F) Optical isometric view of the tube. (G) Peak, (H) peak—valley—peak, and (I) valley of the enhanced tube showing conformality of the Al etching.

nanoparticle deposition. Figure 6D demonstrates SEM images after application of the developed etching fabrication procedure for four additional aluminum grades—Al 1100, Al 3003, Al 5052, and Al 7075. The formation of microstructures similar to Al 6061 demonstrates the applicability of the process to a wide variety of commercially available aluminum grades.

Improvement in thermal performance attributed to an increase in surface area, and earlier flow regime transitions have been previously demonstrated in extruded axial and helical grooved tubes. While such methods are inherently associated with significantly higher manufacturing costs, microstructuring these tubes can lead to improved heat transfer performance when compared to off-the-shelf alter-

natives. To examine the applicability of our fabrication procedure to such tubes as well as to demonstrate the highly conformal nature of Al etching, we etch existing axial grooved tubes (Figure 6E,F). SEM analysis (Figure 6G–I) demonstrated that Al microstructuring occurred at both the valley and the peak of grooves, thereby demonstrating conformal coating on more expensive and intricate internal features.

Although demonstrated here as a candidate for enhancing flow boiling in metallic tubes prevalent in many realistic systems, additional work is needed on multiple fronts to further enhance the penetration of crystallographic etching to real-life applications. Future work dedicated to flow boiling tests in enhanced tubes that are subsequently microstructured

can help examine heat transfer enhancement and the possibility of reduction in manufacturing costs associated with drawn and welded tubes. In addition, thermal performance of such microstructures with working fluids possessing differing thermophysical properties such as zeotropic refrigerant blends and low global warming potential refrigerants need to be studied. Furthermore, the presence of compressor oil in the majority of vapor compression systems for lubrication purposes justifies examining heat transfer effects in etched tubing at different oil in circulation ratios. While such flow boiling enhancements in the refrigerant side of a heat exchanger are noteworthy, more work also needs to be done in analyzing the overall system level performance during heat exchange with secondary working fluids such as ethylene glycol or air. The overall heat transfer impact is expected to be lower due to the added resistances brought forth by the secondary fluids. From a structure length-scale standpoint, the investigation of optimum length scales required to delay dry-out during refrigerant flow boiling is an area that could benefit the research community. From a manufacturing standpoint, future work devoted to structure integrity after tube expansion to attach fins is warranted due to the heavy use of refrigerant flow boiling in evaporators having air-side heat transfer. In addition, more work needs to be dedicated to durability studies for a range of mass flux and structure length scales. Finally, the effects of structured flow boiling performance with alternate working fluids, tube orientations, varying channel diameters, and varying inlet test conditions as well as in the presence of particulate fouling present possible future avenues for inquest.

CONCLUSIONS

In summary, a simple, ultrascalable, cost-effective, and durable method for flow boiling enhancement in arbitrarily shaped and long, conventional Al tubes with refrigerant as the working fluid has been developed. Flow boiling heat transfer experiments were performed in structured tubes, ranging from the micrometer to nanometer scale in feature height and cavity size and compared with plain tubes. A significant increase in the average heat transfer coefficient is reported for the microstructured etched tubes owing to an increase in nucleation cavities of the desirable size range, enhanced turbulence at higher mass flux cases, and a thinner liquid film in the stratified and annular flow regimes. While these microstructures do exhibit an increased pressure drop, enhancement factors greater than 2 underlines the much greater heat transfer improvement when compared to the added pumping cost. To examine commercial applicability, a 28-day durability study was performed with etched Al tubes demonstrating steady heat transfer results with negligible performance impact. Finally, to demonstrate the coating method in existing industrially relevant tubes and to measure coating conformality, we apply the etching approach on commercial low-finned Al tubing with exceptional results.

METHODS

Experimental Facility. The schematic and photograph of the experimental setup are shown in Figure 3A,B, respectively. A variable frequency gear pump is used for circulating the refrigerant through the flow loop, regulating the mass flux in the test section. The mass flow rate is measured with a Coriolis flowmeter, placed at the exit of the pump. The flow then passes through a preheater to control the inlet conditions into the test section, which is maintained at $1-2\,^{\circ}\text{C}$ below the saturation temperature. The preheater consists of a 500 W rope

heater wound around a 1.8 m long copper tube with a 6.023 mm inner diameter. The heat added to the flow in the preheater is controlled with a variac power supply. The refrigerant is then routed to the test section, details of which can be found in Section S4. After the test section, the saturated refrigerant passes through a brazed plate heat exchanger coupled to an ethylene glycol chiller and is fully condensed, so it can safely be returned to the pump. The refrigerant temperature and pressure are measured in a variety of locations throughout the flow loop to define thermodynamic states. Resistance temperature detectors are used to measure the test section inlet and outlet temperatures, and calibrated T-type thermocouples are used for all other measurements in the loop. The system pressure is regulated with a piston cylinder and continually measured with piezoresistive pressure transducers. The entire facility is insulated to minimize heat loss to the ambient. All data were recorded at steady state using a National Instruments Data Acquisition System with LabVIEW.

ASSOCIATED CONTENT

Supporting Information

The Supporting Information is available free of charge at https://pubs.acs.org/doi/10.1021/acsanm.1c00524.

Additional information on fabrication materials (Section S1); video S1 (Section S2); characterization (Section S3); test section (Section S4); data reduction (Section S5); facility validation (S6); heat flux vs wall superheat curves (Section S7); cavity size (Section S8); flow regime map (Section S9); contact angle measurements (Section S10); liquid film thickness and turbulence (Section S11) (PDF)

Flow regime visualization at test-section exit (Video S1) (MP4)

AUTHOR INFORMATION

Corresponding Authors

Anthony M. Jacobi — Department of Mechanical Science and Engineering, University of Illinois at Urbana—Champaign, Urbana, Illinois 61801, United States; Email: a-jacobi@illinois.edu

Nenad Miljkovic — Department of Mechanical Science and Engineering, University of Illinois at Urbana—Champaign, Urbana, Illinois 61801, United States; Materials Research Laboratory, University of Illinois at Urbana—Champaign, Urbana, Illinois 61801, United States; Department of Electrical and Computer Engineering, University of Illinois, Urbana, Illinois 61801, United States; International Institute for Carbon Neutral Energy Research (WPI-I2CNER), Kyushu University, Fukuoka 819-0395, Japan; orcid.org/0000-0002-0866-3680; Email: nmiljkov@illinois.edu

Authors

Nithin Vinod Upot — Department of Mechanical Science and Engineering, University of Illinois at Urbana—Champaign, Urbana, Illinois 61801, United States; orcid.org/0000-0002-0088-6273

Allison Mahvi — Department of Mechanical Science and Engineering, University of Illinois at Urbana—Champaign, Urbana, Illinois 61801, United States; National Renewable Energy Laboratory, Golden, Colorado 15013, United States

Kazi Fazle Rabbi — Department of Mechanical Science and Engineering, University of Illinois at Urbana—Champaign, Urbana, Illinois 61801, United States; occid.org/0000-0003-3630-1625

Jiaqi Li – Department of Mechanical Science and Engineering, University of Illinois at Urbana–Champaign, Urbana, Illinois 61801, United States; o orcid.org/0000-0002-3218-5930

Complete contact information is available at: https://pubs.acs.org/10.1021/acsanm.1c00524

Author Contributions

[#]A.M. and K.F.R. contributed equally to this work.

Notes

The authors declare no competing financial interest.

ACKNOWLEDGMENTS

N.M. and A.M.J. gratefully acknowledge funding support from the Office of Naval Research (ONR) under Grant nos. N00014-16-1-2625 and N00014-21-1-2089. All of the authors gratefully acknowledge funding support from the Air Conditioning and Refrigeration Center (ACRC) and the Center for Integrated Thermal Management of Aerospace Systems (CITMAV). N.M. gratefully acknowledges funding support from the International Institute for Carbon Neutral Energy Research (WPI-I2CNER), sponsored by the Japanese Ministry of Education, Culture, Sports, Science and Technology. The authors thank Scot Regan and Matthew Baker of Brazeway for providing them with commercial Al hairpin tubing for commercial enhanced tubing demonstration studies. The authors thank Dr. Richard T. Haasch and Dr. Kathy Walsh at the Materials Research Laboratory, University of Illinois, for their assistance in materials characterization and insightful discussion.

REFERENCES

- (1) Agonafer, D.; Spector, M. S.; Miljkovic, N. Materials and Interface Challenges in High Vapor Quality Two-Phase Flow Boiling Research. *IEEE Trans. Compon., Packag., Manuf. Technol.* **2021**, in press. DOI: 10.1109/TCPMT.2021.3085255.
- (2) Armarego, W. L. Purification of Laboratory Chemicals; Butterworth-Heinemann, 2017.
- (3) Earle, M. J.; Esperança, J. M.; Gilea, M. A.; Lopes, J. N. C.; Rebelo, L. P.; Magee, J. W.; Seddon, K. R.; Widegren, J. A. The Distillation and Volatility of Ionic Liquids. *Nature* **2006**, *439*, 831–834.
- (4) Bose, S.; Kuila, T.; Nguyen, T. X. H.; Kim, N. H.; Lau, K.-T.; Lee, J. H. Polymer Membranes for High Temperature Proton Exchange Membrane Fuel Cell: Recent Advances and Challenges. *Prog. Polym. Sci.* **2011**, *36*, 813–843.
- (5) El-Dessouky, H. T.; Ettouney, H. M. Fundamentals of Salt Water Desalination; Elsevier, 2002.
- (6) Kalogirou, S. A. Seawater Desalination Using Renewable Energy Sources. Prog. Energy Combust. Sci. 2005, 31, 242–281.
- (7) Beér, J. M. High Efficiency Electric Power Generation: The Environmental Role. *Prog. Energy Combust. Sci.* **2007**, 33, 107–134.
- (8) Hung, T.-C.; Shai, T.; Wang, S. K. A Review of Organic Rankine Cycles (ORCs) for the Recovery of Low-Grade Waste Heat. *Energy* **1997**, 22, 661–667.
- (9) Dincer, I.; Kanoglu, M. Refrigeration Systems and Applications, Vol. 2; Wiley Online Library, 2010.
- (10) Arora, C. P. Refrigeration and Air Conditioning; Tata McGraw-Hill Education, 2000.
- (11) Collaudin, B.; Rando, N. Cryogenics in Space: A Review of the Missions and of the Technologies. *Cryogenics* **2000**, *40*, 797–819.
- (12) Mousa, M. H.; Miljkovic, N.; Nawaz, K. Review of Heat Transfer Enhancement Techniques for Single Phase Flows. *Renewable Sustainable Energy Rev.* **2021**, *137*, No. 110566.
- (13) Saitoh, S.; Daiguji, H.; Hihara, E. Effect of Tube Diameter on Boiling Heat Transfer of R-134a in Horizontal Small-Diameter Tubes. *Int. J. Heat Mass Transfer* **2005**, *48*, 4973–4984.

- (14) Baliga, B. J. Gallium Nitride and Silicon Carbide Power Devices; World Scientific Publishing Company, 2016.
- (15) Pengelly, R. S.; Wood, S. M.; Milligan, J. W.; Sheppard, S. T.; Pribble, W. L. A Review of GaN on SiC High Electron-Mobility Power Transistors and MMICs. *IEEE Trans. Microwave Theory Tech.* **2012**, *60*, 1764–1783.
- (16) Wei, J. Challenges in Cooling Design of CPU Packages for High-Performance Servers. *Heat Transfer Eng.* **2008**, *29*, 178–187.
- (17) Kimura, T.; Nakamoto, T.; Mizuno, M.; Araki, H. Effect of Silicon Content on Densification, Mechanical and Thermal Properties of Al-xSi Binary Alloys Fabricated Using Selective Laser Melting. *Mater. Sci. Eng.* **2017**, *682*, 593–602.
- (18) Miljkovic, N.; Enright, R.; Nam, Y.; Lopez, K.; Dou, N.; Sack, J.; Wang, E. N. Jumping-Droplet-Enhanced Condensation on Scalable Superhydrophobic Nanostructured Surfaces. *Nano Lett.* **2013**, *13*, 179–187.
- (19) Oh, J.; Birbarah, P.; Foulkes, T.; Yin, S. L.; Rentauskas, M.; Neely, J.; Pilawa-Podgurski, R. C.; Miljkovic, N. Jumping-Droplet Electronics Hot-Spot Cooling. *Appl. Phys. Lett.* **2017**, *110*, No. 123107.
- (20) Li, D.; Wu, G.; Wang, W.; Wang, Y.; Liu, D.; Zhang, D.; Chen, Y.; Peterson, G.; Yang, R. Enhancing Flow Boiling Heat Transfer in Microchannels for Thermal Management with Monolithically-Integrated Silicon Nanowires. *Nano Lett.* **2012**, *12*, 3385–3390.
- (21) Zhu, Y.; Antao, D. S.; Chu, K.-H.; Chen, S.; Hendricks, T. J.; Zhang, T.; Wang, E. N. Surface Structure Enhanced Microchannel Flow Boiling. *J. Heat Transfer* **2016**, *138*, No. 091501.
- (22) Shin, S.; Choi, G.; Kim, B. S.; Cho, H. H. Flow Boiling Heat Transfer on Nanowire-Coated Surfaces with Highly Wetting Liquid. *Energy* **2014**, *76*, 428–435.
- (23) Yang, F.; Li, W.; Dai, X.; Li, C. Flow Boiling Heat Transfer of HFE-7000 in Nanowire-coated Microchannels. *Appl. Therm. Eng.* **2016**, 93, 260–268.
- (24) Sun, B.; Yang, D. Flow Boiling Heat Transfer Characteristics of Nano-Refrigerants in a Horizontal Tube. *Int. J. Refrig.* **2014**, *38*, 206–214
- (25) Sheikholeslami, M.; Rezaeianjouybari, B.; Darzi, M.; Shafee, A.; Li, Z.; Nguyen, T. K. Application of Nano-Refrigerant for Boiling Heat Transfer Enhancement Employing an Experimental Study. *Int. J. Heat Mass Transfer* **2019**, *141*, 974–980.
- (26) Peng, H.; Ding, G.; Jiang, W.; Hu, H.; Gao, Y. Heat Transfer Characteristics of Refrigerant-Based Nanofluid Flow Boiling Inside a Horizontal Smooth Tube. *Int. J. Refrig.* **2009**, 32, 1259–1270.
- (27) Sun, Z.-C.; Ma, X.; Ma, L.-X.; Li, W.; Kukulka, D. J. Flow Boiling Heat Transfer Characteristics in Horizontal, Three-Dimensional Enhanced Tubes. *Energies* **2019**, *12*, No. 927.
- (28) Dawidowicz, B.; Cieśliński, J. T.; Transfer, H. Pressure Drop during Flow Boiling of Pure Refrigerants and Refrigerant/Oil Mixtures in Tube with Porous coating. *Int. J. Heat Mass Transfer* **2012**, *55*, 2549–2558.
- (29) Kaya, A.; Demiryürek, R.; Armağan, E.; Ozaydin-Ince, G.; Sezen, M.; Koşar, A. Boiling Heat Transfer Enhancement in Mini/Microtubes via Polyhydroxyethylmethacrylate (pHEMA) Coatings on Inner Microtube Walls at High Mass Fluxes. *J. Micromech. Microeng.* **2013**, *23*, No. 115017.
- (30) Çıkım, T.; Armağan, E.; Ozaydin Ince, G.; Koşar, A. Flow Boiling Enhancement in Microtubes with Crosslinked pHEMA Coatings and the Effect of Coating Thickness. *J. Heat Transfer* **2014**, *136*, No. 081504.
- (31) Bai, P.; Tang, T.; Tang, B. Enhanced Flow Boiling in Parallel Microchannels with Metallic Porous Coating. *Appl. Therm. Eng.* **2013**, 58, 291–297.
- (32) Morshed, A.; Paul, T. C.; Khan, J. Effect of Cu-Al2O3 Nanocomposite Coating on Flow Boiling Performance of a Microchannel. *Appl. Therm. Eng.* **2013**, *51*, 1135–1143.
- (33) Khanikar, V.; Mudawar, I.; Fisher, T. Effects of Carbon Nanotube Coating on Flow Boiling in a Micro-channel. *Int. J. Heat Mass Transfer* **2009**, *52*, 3805–3817.

- (34) Singh, N.; Sathyamurthy, V.; Peterson, W.; Arendt, J.; Banerjee, D. Flow Boiling Enhancement on a Horizontal Heater using Carbon Nanotube Coatings. *Int. J. Heat Fluid Flow* **2010**, *31*, 201–207.
- (35) Oudah, S. K.; Fang, R.; Tikadar, A.; Salman, A. S.; Khan, J. A. An Experimental Investigation of the Effect of Multiple Inlet Restrictors on the Heat Transfer and Pressure Drop in a Flow Boiling Microchannel Heat Sink. *Int. J. Heat Mass Transfer* **2020**, *153*, No. 119582.
- (36) Khodakarami, S.; Zhao, H.; Rabbi, K. F.; Miljkovic, N. Scalable Corrosion-Resistant Coatings for Thermal Applications. *ACS Appl. Mater. Interfaces* **2021**, *13*, 4519–4534.
- (37) Sarwar, M. S.; Jeong, Y. H.; Chang, S. H. Subcooled Flow Boiling CHF Enhancement with Porous Surface Coatings. *Int. J. Heat Mass Transfer* **2007**, *50*, 3649–3657.
- (38) Baytekin-Gerngross, M.; Gerngross, M.; Carstensen, J.; Adelung, R. Making Metal Surfaces Strong, Resistant, and Multifunctional by Nanoscale-Sculpturing. *Nanoscale Horiz.* **2016**, 1, 467–472.
- (39) Rabbi, K. F.; Boyina, K. S.; Su, W.; Sett, S.; Thamban, A.; Shahane, S.; Wang, S.; Miljkovic, N. Wettability-defined Frosting Dynamics Between Plane Fins in Quiescent Air. *Int. J. Heat Mass Transfer* **2021**, *164*, No. 120563.
- (40) Ma, J.; Cahill, D. G.; Miljkovic, N. Condensation Induced Blistering as a Measurement Technique for the Adhesion Energy of Nanoscale Polymer Films. *Nano Lett.* **2020**, *20*, 3918–3924.
- (41) Chu, K.-H.; Soo Joung, Y.; Enright, R.; Buie, C. R.; Wang, E. N. Hierarchically Structured Surfaces for Boiling Critical Heat Flux Enhancement. *Appl. Phys. Lett.* **2013**, *102*, No. 151602.
- (42) Mehendale, S.; Jacobi, A.; Shah, R. Fluid Flow and Heat Transfer at Micro-and Meso-scales with Application to Heat Exchanger Design. *Appl. Mech. Rev.* **2000**, *53*, 175–193.
- (43) Kew, P. A.; Cornwell, K. Correlations for the Prediction of Boiling Heat Transfer in Small-diameter Channels. *Appl. Therm. Eng.* **1997**, *17*, 705–715.
- (44) Kandlikar, S. G. Fundamental Issues Related to Flow Boiling in Minichannels and Microchannels. *Exp. Therm Fluid Sci.* **2002**, *26*, 389–407.
- (45) Mahvi, A. J.; Boyina, K.; Musser, A.; Elbel, S.; Miljkovic, N. Superhydrophobic Heat Exchangers Delay Frost Formation and Enhance Efficiency of Electric Vehicle Heat Pumps. *Int. J. Heat Mass Transfer* **2021**, 172, No. 121162.
- (46) Cooper, M. Flow Boiling—The 'Apparently Nucleate' Regime. Int. J. Heat Mass Transfer 1989, 32, 459–464.
- (47) Hsu, Y. On The Size Range of Active Nucleation Cavities on a Heating Surface. *J. Heat Transfer* **1962**, *84*, No. 207.
- (48) Sajjad, U.; Sadeghianjahromi, A.; Ali, H. M.; Wang, C.-C. Enhanced Pool Boiling of Dielectric and Highly Wetting Liquids-A Review on Enhancement Mechanisms. *Int. Commun. Heat Mass Transfer* **2020**, *119*, No. 104950.
- (49) Thorncroft, G.; Klausner, J.; Mei, R. Suppression of Flow Boiling Nucleation. J. Heat Transfer 1997, 119, No. 517.
- (50) Saisorn, S.; Kaew-On, J.; Wongwises, S. Flow Pattern and Heat Transfer Characteristics of R-134a Refrigerant During Flow Boiling in a Horizontal Circular Mini-channel. *Int. J. Heat Mass Transfer* **2010**, 53, 4023–4038.
- (51) Jabardo, J. M. S.; Bandarra Filho, E. P. Convective Boiling of Halocarbon Refrigerants Flowing in a Horizontal Copper Tube—An Experimental Study. *Exp. Therm Fluid Sci.* **2000**, 23, 93–104.
- (\$2) Ong, C. L.; Thome, J. Macro-to-microchannel Transition in Two-phase Flow: Part 1—Two-phase flow patterns and film thickness measurements. *Exp. Therm Fluid Sci.* **2011**, *35*, 37–47.
- (53) Ong, C.; Thome, J. Macro-to-microchannel Transition in Two-phase flow: Part 2—Flow boiling heat transfer and critical heat flux. *Exp. Therm Fluid Sci.* **2011**, *35*, 873—886.
- (\$4) Li, J.; Kang, D.; Rabbi, K. F.; Fu, W.; Yan, X.; Fang, X.; Fan, L.; Miljkovic, N. Liquid Film-induced Critical Heat Flux Enhancement on Structured Surfaces. *Sci. Adv.* **2021**, *7*, eabg4537.
- (55) Li, J.; Fu, W.; Zhang, B.; Zhu, G.; Miljkovic, N. Ultrascalable Three-Tier Hierarchical Nanoengineered Surfaces for Optimized Boiling. *ACS Nano* **2019**, *13*, 14080–14093.

- (56) Suszko, A.; El-Genk, M. S. Saturation boiling of PF-5060 on rough Cu surfaces: Bubbles Transient Growth, Departure Diameter and Detachment Frequency. *Int. J. Heat Mass Transfer* **2015**, *91*, 363–373
- (57) Bloch, G.; Sattelmayer, T. Effects of Turbulence and Secondary Flows on Subcooled Flow Boiling. *Heat Mass Transfer* **2014**, *50*, 427–435.
- (58) Yang, F.; Dai, X.; Peles, Y.; Cheng, P.; Khan, J.; Li, C. Flow Boiling Phenomena in a Single Annular Flow Regime in Microchannels (I): Characterization of Flow Boiling Heat Transfer. *Int. J. Heat Mass Transfer* **2014**, *68*, 703–715.
- (59) Wong, K.; Leong, K. Nucleate Flow Boiling Enhancement on Engineered Three-Dimensional Porous Metallic Structures in FC-72. *Appl. Therm. Eng.* **2019**, *159*, No. 113846.
- (60) Liang, G.; Mudawar, I. Review of Nanoscale Boiling Enhancement Techniques and Proposed Systematic Testing Strategy to Ensure Cooling Reliability and Repeatability. *Appl. Therm. Eng.* **2020**, *184*, No. 115982.
- (61) Yang, C.-M.; Hrnjak, P. Effect of Helical Micro-Fins on Two-Phase Flow Behavior of R410A Evaporating in Horizontal Round Tubes Obtained Through Visualization. *Int. J. Heat Mass Transfer* **2019**, *144*, No. 118654.